probably would not be a straight line, and the antenna would probably be programmed to point at the apparent receiver or transmitter. This can be taken into account by a rotation of coordinates in reference frame S.

References

[1] A. V. Balakrishman, *Space Communications*. New York: McGraw-Hill, 1963, p. 29.
[2] W. K. H. Panofsky and M. Phillips, *Classical Electricity and Magnetism*. Reading, Mass.: Addison-Wesley, 1955.
[3] J. D. Jackson, *Classical Electrodynamics*. New York: Wiley, 1962.
[4] L. D. Landau and E. M. Lifshitz, *The Classical Theory of Fields*. New York: Pergamon, 1962.
[5] H. Fujioka, T. Shiozawa, and N. Kumagai, "Electromagnetic radiation from an electric dipole moving with relativistic velocity," *Proc. Electron. and Commun. Engrs. Japan*, vol. 49, June 1966.
[6] D. F. Lawden, *An Introduction to Tensor Calculus and Relativity*. London: Methuen, 1967, pp. 7–13, 81–89.
[7] R. M. Lewis and W. Pressman, "Radiation and propagation of electromagnetic waves from moving sources," *Radio Sci.*, vol. 1, pp. 1029–1040, September 1966.

Radiation from a Circularly Polarized Antenna Through the Ionized Wake of a Mars-Entry Capsule

RICHARD WOO, MEMBER, IEEE, AND AKIRA ISHIMARU, SENIOR MEMBER, IEEE

Abstract—**The effects of the ionized wake of a Mars-entry capsule on radiation from a circularly polarized antenna operating at 400 and 2295 MHz are studied. The circularly polarized antenna is represented by a turnstile antenna $\lambda/4$ above a ground plane, while the ionized wake is approximated by a cylindrically stratified plasma consisting of N-plasma regions. Integral expressions for the fields are obtained for the antenna located in the wake and are evaluated using saddle-point integration to yield the radiation patterns. Computed patterns for the two simplest configurations $N = 1$ and $N = 2$ are presented. The radiation patterns for both near- and far-wake electron-density profiles develop a conical null region whose extent is proportional to the peak electron density in the wake. For the near-wake electron-density profile, sharp peaks which are attributable to leaky-wave radiation, appear within the null region of the patterns. The effect of the conical null region in the patterns is to prolong blackout time for communication cone angles that lie within the null region. There are no serious depolarization effects in the nonnull region and satisfactory communications can be carried out.**

I. Introduction

DURING the entry of a blunt-body capsule into the Martian atmosphere a plasma will surround and trail the capsule. The antenna for a mission of this type is located in the aft portion of the capsule and propagation takes place through the ionized wake. The capsule diameter in presently conceived designs for Mars-entry capsules is approximately 175 cm, and communications links with frequencies of 400 and 2295 MHz are planned. Blackout will occur at both frequencies [1]. The purpose of this paper is to investigate the effects of the ionized wake on communications prior to and after blackout. The antenna is circularly polarized and will be represented by a turnstile antenna $\lambda/4$ above a ground plane.

The plasma properties of the ionized wake must be known before the effects of the ionized wake can be considered. Determination of these properties is a formidable problem by itself, because it involves a detailed knowledge of aerodynamic flow fields and flow rates which, in turn, are dependent on the environment in which the capsule is moving. Nevertheless, a reasonable representation of the ionized wake can be made.

Since the plasma associated with Martian entry has a low temperature of ~800–1300° K [2] and is weakly ionized, the magnetoionic theory description of the plasma is assumed. No static magnetic field is present in the vicinity of Mars and the plasma is also isotropic [3]. Furthermore, the electron-neutral collision frequency is at least three orders of magnitude lower than the electron plasma frequency and collision losses can be neglected [1]. Since the electron-density profiles in the wake are axisymmetric, the ionized wake will be represented by a cylindrically stratified plasma. In the near-wake region, electron density increases at first and then decreases in the radial direction, with the maximum occurring near the edge of the wake while in the far-wake region electron density is maximum on axis and decreases in the radial direction [4]. Both types of electron-density profiles will therefore be approximated.

In this paper the fields are solved for a horizontal electric dipole located in a cylindrically stratified plasma con-

Manuscript received November 29, 1968; revised March 13, 1969. This research was sponsored by NASA under Contract NAS 7-100.
R. Woo is with the Jet Propulsion Laboratory, California Institute of Technology, Pasadena, Calif.
A. Ishimaru is with the University of Washington, Seattle, Wash., and is a Consultant to the Jet Propulsion Laboratory.

sisting of N-plasma regions. Circularly polarized radiation patterns for a turnstile antenna $\lambda/4$ above a ground plane in configurations of one and two regions of cylindrically stratified plasma are then presented and discussed.

II. Integral Formulation of Fields for Horizontal Dipole

The plasma configuration is shown in Fig. 1. The regions are numbered i, where $i = 1,2,3, \cdots, N+1$. Region $N+1$ is free space. We will denote the outer radius of region i by ρ_i. For other quantities, the subscript i will be used to refer them to region i.

The free-space region $i = N+1$ is characterized by permittivity ϵ_0 and permeability μ_0. According to the magnetoionic theory description for a homogeneous isotropic and lossless plasma, the plasma region i is represented by a medium whose permittivity ϵ_i is given [5] by

$$\epsilon_i = \left[1 - \left(\frac{\omega_{pi}}{\omega}\right)^2\right]\epsilon_0 \tag{1}$$

$$\omega_{pi}^2 = \frac{n_i e^2}{m\epsilon_0} \tag{2}$$

where n_i is the electron density, e is the electron charge, m is the electron mass, and ω_{pi} is the electron plasma frequency. The propagation constant of region i, k_i is then given by $k_i^2 = \omega^2\mu_0\epsilon_i$.

Assuming a time dependence of $e^{j\omega t}$, the respective electric and magnetic field intensities, $\boldsymbol{E}$ and $\boldsymbol{H}$ are related to the electric π and magnetic π^* Hertz potentials through the following equations

$$\boldsymbol{E} = \nabla \times \nabla \times \pi - j\omega\mu_0 \nabla \times \pi^* \tag{3}$$

$$\boldsymbol{H} = \nabla \times \nabla \times \pi^* + j\omega\epsilon \nabla \times \pi \tag{4}$$

where ϵ is the intrinsic permittivity of the medium.

The electric dipole of moment Il is assumed to be located at ρ_0,ϕ_0,z_0 and oriented in the x direction in plasma region m (see Fig. 1). The x component of π, π_{xm} will therefore represent the primary field and satisfy the following equation

$$(\nabla^2 + k_m^2)\pi_{xm} = -\frac{Il}{j\omega\epsilon_m}\delta(\phi - \phi_0)\delta(z - z_0)\delta(\rho - \rho_0)/\rho \tag{5}$$

where δ is the Dirac delta function and subscript m refers to the region m. Since both E_z and H_z will be present in the secondary fields, the respective z components of π and π^*, π_{zi} and π_{zi}^* will be used for region i. π_{zi} and π_{zi}^* will satisfy the following wave equations

$$(\nabla^2 + k_i^2)\pi_{zi} = 0 \tag{6}$$

$$(\nabla^2 + k_i^2)\pi_{zi}^* = 0. \tag{7}$$

Integral representations for the Hertz potentials can be written using a Fourier integral in the z direction and a Fourier series in the ϕ direction [6]. For the primary field in region m we have

$$\pi_{xm} = \frac{Il}{j\omega\epsilon_m}\frac{1}{8\pi j}\sum_{n=-\infty}^{\infty}\int_{-\infty}^{\infty} H_n^{(2)}(\lambda_m\rho) \cdot J_n(\lambda_m\rho_0)\, e^{-jn(\phi-\phi_0)} e^{-jh(z-z_0)}\, dh \tag{8}$$

where

$$\lambda_m^2 = k_m^2 - h^2.$$

J_n is the nth order Bessel function of the first kind and $H_n^{(2)}$ the nth order Hankel function of the second kind. Equation (8) is for $\rho > \rho_0$; when $\rho < \rho_0$, ρ and ρ_0 must be interchanged in the equation. For the secondary fields we have the following results for region i:

$$\pi_{zi} = \sum_{n=-\infty}^{\infty}\int_{-\infty}^{\infty}\left[a_n^{(i)}J_n(\lambda_i\rho) + c_n^{(i)}H_n^{(2)}(\lambda_i\rho)\right] \cdot e^{-jn\phi}e^{-jh(z-z_0)}\, dh \tag{9}$$

$$\pi_{zi}^* = \sum_{n=-\infty}^{\infty}\int_{-\infty}^{\infty}\left[b_n^{(i)}J_n(\lambda_i\rho) + d_n^{(i)}H_n^{(2)}(\lambda_i\rho)\right] \cdot e^{-jn\phi}e^{-jh(z-z_0)}\, dh \tag{10}$$

where

$$\lambda_i^2 = k_i^2 - h^2.$$

The superscript i in the coefficients a_n, b_n, c_n, and d_n refers to the fields in region i. Since the fields are finite at $\rho = 0$, $c_n^{(1)} = d_n^{(1)} = 0$. Also, since we have outgoing waves in the free space region $i = N+1$, $a_n^{(N+1)} = b_n^{(N+1)} = 0$.

The cylindrical components of $\boldsymbol{E}$ and $\boldsymbol{H}$ for region i can be obtained using (3) and (4). We have

$$E_{zi} = \left(\frac{\partial^2}{\partial z^2} + k_i^2\right)\pi_{zi} \tag{11}$$

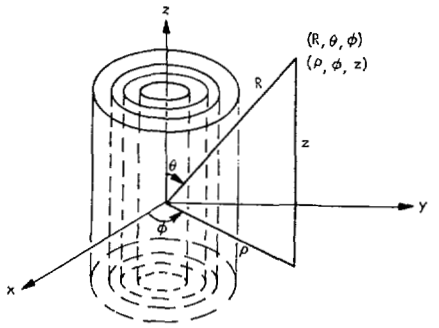

(a)

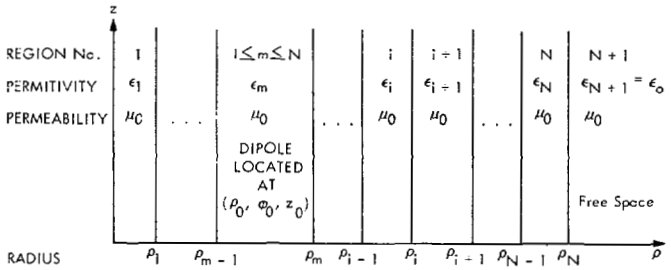

(b)

Fig. 1. Geometry of problem.

$$E_{\phi i} = \frac{1}{\rho}\frac{\partial^2 \pi_{zi}}{\partial \phi \partial z} + j\omega\mu_0 \frac{\partial \pi_{zi}^*}{\partial \rho} \tag{12}$$

$$E_{\rho i} = \frac{\partial^2 \pi_{zi}}{\partial \rho \partial z} - \frac{j\omega\mu_0}{\rho}\frac{\partial \pi_{zi}^*}{\partial \phi} \tag{13}$$

$$H_{zi} = \left(\frac{\partial^2}{\partial z^2} + k_i^2\right)\pi_{zi}^* \tag{14}$$

$$H_{\phi i} = \frac{1}{\rho}\frac{\partial^2 \pi_{zi}^*}{\partial \phi \partial z} - j\omega\epsilon_i \frac{\partial \pi_{zi}}{\partial \rho} \tag{15}$$

$$H_{\rho i} = \frac{\partial^2 \pi_{zi}^*}{\partial \rho \partial z} + \frac{j\omega\epsilon_i}{\rho}\frac{\partial \pi_{zi}}{\partial \phi}. \tag{16}$$

In region m we have the following additional components due to the primary field

$$E_{zm} = \frac{\partial^2 \pi_{xm}}{\partial z \partial \rho}\cos\phi - \frac{1}{\rho}\frac{\partial^2 \pi_{xm}}{\partial z \partial \phi}\sin\phi \tag{17}$$

$$E_{\phi m} = \left(\frac{\partial^2 \pi_{xm}}{\partial z^2} + \frac{\partial^2 \pi_{xm}}{\partial \rho^2}\right)\sin\phi + \frac{\partial}{\partial \rho}\left(\frac{1}{\rho}\frac{\partial \pi_{xm}}{\partial \phi}\right)\cos\phi \tag{18}$$

$$E_{\rho m} = \left(\frac{1}{\rho^2}\frac{\partial \pi_{xm}}{\partial \phi} - \frac{1}{\rho}\frac{\partial^2 \pi_{xm}}{\partial \phi \partial \rho}\right)\sin\phi - \left(\frac{1}{\rho}\frac{\partial \pi_{xm}}{\partial \rho} + \frac{1}{\rho^2}\frac{\partial^2 \pi_{xm}}{\partial \phi^2} + \frac{\partial^2 \pi_{xm}}{\partial z^2}\right)\cos\phi \tag{19}$$

$$H_{zm} = -j\omega\epsilon_m \frac{\partial \pi_{xm}}{\partial \rho}\sin\phi - j\omega\epsilon_m \frac{1}{\rho}\left(\frac{\partial \pi_{xm}}{\partial \phi}\right)\cos\phi \tag{20}$$

$$H_{\phi m} = j\omega\epsilon_m \frac{\partial \pi_{xm}}{\partial z}\cos\phi \tag{21}$$

$$H_{\rho m} = j\omega\epsilon_m \frac{\partial \pi_{xm}}{\partial z}\sin\phi. \tag{22}$$

The boundary conditions at ρ_i require that the tangential $\boldsymbol{E}$ and $\boldsymbol{H}$ fields be continuous. Imposing these boundary conditions at each boundary ρ_i yields the following results in matrix form

$$\begin{bmatrix} 0 \\ 0 \\ c_n^{(N+1)} \\ d_n^{(N+1)} \end{bmatrix} = M_n^{(N)} \cdot M_n^{(N-1)} \cdots M_n^{(1)} \begin{bmatrix} a_n^{(1)} \\ b_n^{(1)} \\ 0 \\ 0 \end{bmatrix} - M_n^{(N)} \cdot M_n^{(N-1)} \cdots M_n^{(m+1)} \left\{ [B_n^{(m)}]^{-1} \begin{bmatrix} \gamma_n^{(m)} \\ \eta_n^{(m)} \\ \alpha_n^{(m)} \\ \beta_n^{(m)} \end{bmatrix} - M_n^{(m)} [B_n^{(m-1)}]^{-1} \begin{bmatrix} \gamma_n^{(m-1)} \\ \eta_n^{(m-1)} \\ \alpha_n^{(m-1)} \\ \beta_n^{(m-1)} \end{bmatrix} \right\} \tag{23}$$

where

$$M_n^{(i)} = [B_n^{(i)}]^{-1} A_n^{(i)}$$

$$A_n^{(i)} = \begin{bmatrix} \lambda_i^2 J_n(\lambda_i\rho_i) & 0 & \lambda_i^2 H_n^{(2)}(\lambda_i\rho_i) & 0 \\ 0 & \lambda_i^2 J_n(\lambda_i\rho_i) & 0 & \lambda_i^2 H_n^{(2)}(\lambda_i\rho_i) \\ (-nh/\rho_i) J_n(\lambda_i\rho_i) & j\omega\mu_0\lambda_i J_n'(\lambda_i\rho_i) & (-nh/\rho_i) H_n^{(2)}(\lambda_i\rho_i) & j\omega\mu_0\lambda_i H_n^{(2)\prime}(\lambda_i\rho_i) \\ -j\omega\epsilon_i\lambda_i J_n'(\lambda_i\rho_i) & (-nh/\rho_i) J_n(\lambda_i\rho_i) & -j\omega\epsilon_i\lambda_i H_n^{(2)\prime}(\lambda_i\rho_i) & (-nh/\rho_i) H_n^{(2)}(\lambda_i\rho_i) \end{bmatrix}.$$

$B_n^{(i)}$ is similar to $A_n^{(i)}$ except that λ_i and ϵ_i are replaced by λ_{i+1} and ϵ_{i+1}, respectively, and $[B_n^{(0)}]^{-1} = 0$:

$$\gamma_n^{(m)} = -\frac{Il}{4\pi}\omega\mu_0 \frac{jh\lambda_m}{4k_m^2}\left[e^{j(n+1)\phi_0} J_{n+1}(\lambda_m\rho_0) - e^{j(n-1)\phi_0} J_{n-1}(\lambda_m\rho_0)\right] H_n^{(2)}(\lambda_m\rho_m)$$

$$\eta_n^{(m)} = -\frac{Il}{4\pi}\omega\mu_0 \frac{\lambda_m}{4\omega\mu_0}\left[e^{j(n+1)\phi_0} J_{n+1}(\lambda_m\rho_0) + e^{j(n-1)\phi_0} J_{n-1}(\lambda_m\rho_0)\right] H_n^{(2)}(\lambda_m\rho_m)$$

$$\alpha_n^{(m)} = \frac{Il}{4\pi}\omega\mu_0\frac{j}{8k_m^2}\{[(k_m^2+h^2)e^{j(n+1)\phi_0}J_{n+1}(\lambda_m\rho_0) + \lambda_m^2 e^{j(n-1)\phi_0}J_{n-1}(\lambda_m\rho_0)]H_{n+1}^{(2)}(\lambda_m\rho_m) - [(k_m^2+h^2)e^{j(n+1)\phi_0}J_{n-1}(\lambda_m\rho_0) + \lambda_m^2 e^{j(n+1)\phi_0}J_{n+1}(\lambda_m\rho_0)]H_{n-1}^{(2)}(\lambda_m\rho_m)\}$$

$$\beta_n^{(m)} = \frac{Il}{4\pi}\omega\mu_0\frac{h}{4\omega\mu_0}[e^{j(n+1)\phi_0}J_{n+1}(\lambda_m\rho_0)H_{n+1}^{(2)}(\lambda_m\rho_m) + e^{j(n-1)\phi_0}J_{n-1}(\lambda_m\rho_0)H_{n-1}^{(2)}(\lambda_m\rho_m)].$$

$\gamma_n^{(m-1)}$, $\eta_n^{(m-1)}$, $\alpha_n^{(m-1)}$, and $\beta_n^{(m-1)}$ are obtained from $\gamma_n^{(m)}$, $\eta_n^{(m)}$, $\alpha_n^{(m)}$, and $\beta_n^{(m)}$, respectively, by changing ρ_0 to ρ_{m-1} and ρ_m to ρ_0. Equation (23) consists of four equations and four unknown coefficients and can be readily solved. The remaining coefficients are obtained through the following recursion relation

$$\begin{bmatrix} a_n^{(i+1)} \\ b_n^{(i+1)} \\ c_n^{(i+1)} \\ d_n^{(i+1)} \end{bmatrix} = M_n^{(i)} \begin{bmatrix} a_n^{(i)} \\ b_n^{(i)} \\ c_n^{(i)} \\ d_n^{(i)} \end{bmatrix} - [B_n^{(m)}]^{-1} \begin{bmatrix} \gamma_n^{(m)} \\ \eta_n^{(m)} \\ \alpha_n^{(m)} \\ \beta_n^{(m)} \end{bmatrix} \cdot\delta(i-m) + [B_n^{(m-1)}]^{-1} \begin{bmatrix} \gamma_n^{(m-1)} \\ \eta_n^{(m-1)} \\ \alpha_n^{(m-1)} \\ \beta_n^{(m-1)} \end{bmatrix} \cdot\delta(i-m+1). \quad (24)$$

III. Radiation Patterns for Horizontal Dipole

The radiation fields are obtained by using the method of saddle-point integration [7] to evaluate the integral expressions of the fields in free space. The resulting spherical components of the radiation fields are

$$E_\theta = -2k^2\sin\theta e^{jkz_0\cos\theta}\frac{e^{-jkR}}{R}\cdot\sum_{n=-\infty}^{\infty} c_n^{(N+1)}e^{-jn\phi+j(n+1)\pi/2}$$

$$H_\phi = \left(\frac{\epsilon_0}{\mu_0}\right)^{1/2} E_\theta \quad (25)$$

$$E_\phi = 2\omega\mu_0 k\sin\theta e^{jkz_0\cos\theta}\frac{e^{-jkR}}{R}\cdot\sum_{n=-\infty}^{\infty} d_n^{(N+1)}e^{-jn\phi+j(n+1)\pi/2}$$

$$H_\theta = -\left(\frac{\epsilon_0}{\mu_0}\right)^{1/2} E_\phi \quad (26)$$

where k is the free-space wavenumber, $c_n^{(N+1)}$ and $d_n^{(N+1)}$ are given in (23), and

$$\lambda_i^2 = k_i^2 - k^2\cos^2\theta$$

$$h = k\cos\theta.$$

It should be noted that the corresponding modified Bessel functions must be used when $\lambda_i^2 < 0$.

IV. Results and Discussion for Turnstile Antenna

We will consider a turnstile antenna radiating RHCP (right-hand circular polarization) in the z direction. The turnstile antenna consists of crossed dipoles oriented in the x and y directions with the dipole oriented in the y direction fed -90 degrees out of phase with respect to the dipole oriented in the x direction. We will assume that there is an infinite ground plane at $z = 0$ and that the turnstile antenna is located $\lambda/4$ above the ground plane. If the turnstile antenna is located on the z axis, the free-space patterns which will be used for comparison are given by

$$E_{\text{RHCP}} = \frac{Il}{4\pi}\omega\mu_0\sqrt{2}(1+\cos\theta)\sin\left(\frac{\pi}{2}\cos\theta\right)e^{-j\phi}\frac{e^{-jkR}}{R} \quad (27)$$

$$E_{\text{LHCP}} = -\frac{Il}{4\pi}\omega\mu_0\sqrt{2}(1-\cos\theta)\sin\left(\frac{\pi}{2}\cos\theta\right)e^{-j\phi}\frac{e^{-jkR}}{R} \quad (28)$$

where LHCP is left-hand circular polarization. The gain function is

$$G(\theta,\phi) = 4\pi\Psi(\theta,\phi)\Big/\int_0^{2\pi}\int_0^{\pi/2}\Psi(\theta,\phi)\sin\theta\,d\theta\,d\phi \quad (29)$$

where

$$\Psi = |E_{\text{RHCP}}|^2 + |E_{\text{LHCP}}|^2.$$

The absolute gain which is given by $10\log_{10}G(0,0)$ is then 7.1684 dB. The free space patterns for RHCP and LHCP relative to isotropic are shown in Fig. 2. In Fig. 2 as well as in Figs. 3–6, the upper lattern is RHCP while the lower pattern is LHCP.

The effects of the two simplest plasma configurations on the radiation patterns of the turnstile antenna will now be discussed. In Section IV-A the ionized wake is represented by a plasma column ($N = 1$). Yip and Seshadri [8] have recently conducted studies on a similar problem. In the present study there is no magnetic field present but the effects of locating the antenna off axis are included and the circularly polarized patterns presented. In Section IV-B the ionized wake is approximated by two plasma regions ($N = 2$) and we will term this the shell configuration.

A. Column Configuration

The radiation patterns are given in terms of the normalized plasma column radius $k\rho_1$, with $k\rho_1$ assuming values of 10 and 50. Presently conceived designs for Mars-entry capsules utilize communications links whose frequencies are 400 and 2295 MHz. Values of $k\rho_1$ of 10 and 50 correspond to a plasma column radius of the order of 100 cm for 400 and 2295 MHz, respectively.

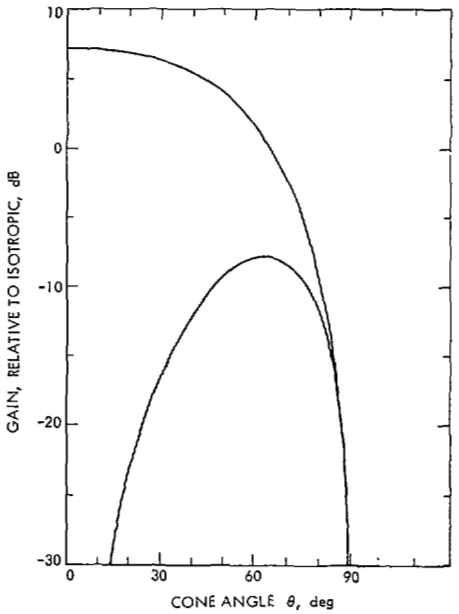

Fig. 2. Free-space patterns for turnstile antenna located $\lambda/4$ above infinite ground plane.

Patterns for the case where the turnstile antenna is located on the z axis are shown in Fig. 3. For this case, only the $n = \pm 1$ terms need be summed in (25) and (26). It can be seen that for both cases of $k\rho_1$ there is an on-axis null and that the extent of this null increases with an increase in electron density. Thus, as the plasma increases in intensity, radiation is increasingly confined in the neighborhood of endfire direction. This behavior of the radiation fields can be explained from simple physical considerations using the geometric-optical approach. If the turnstile antenna is considered as a source emitting rays in all directions in the plasma, the rays are refracted into the free-space region as they reach the free-space interface. Due to Snell's refraction law, there exists a critical angle θ_{cr} which corresponds to a minimum cone angle permissible for the refracted rays in the free-space region. This critical angle is given by $\theta_{cr} = \cos^{-1} \sqrt{\epsilon_1}$. Calculated results of θ_{cr} are shown in Fig. 3, and as would be expected, the larger the $k\rho_1$ the better the correspondence. For cone angles greater than θ_{cr}, the patterns develop peaks whose number increases with $k\rho_1$; this is due to the fact that the fields become more phase sensitive as $k\rho_1$ increases. It is interesting to note that even for intense plasmas the axial ratio does not deteriorate appreciably from that of corresponding cone angles in the free-space patterns.

When the antenna is located off axis, higher order terms than $n = \pm 1$ must be considered in (25) and (26). The series converge when the order of $4k\rho_1$ terms ($| n | < 2k\rho_1$) are summed. The patterns obtained when the antenna is located at a distance equal to half the normalized plasma column radius at $\phi = 0$ degrees are shown in Fig. 4. Shifting the antenna off axis does not have a significant effect on the patterns. As would be expected, the $\phi = 180$ degrees patterns tend towards corresponding ϵ_1 on-axis patterns for larger $k\rho_1$, while the $\phi = 0$ degrees patterns

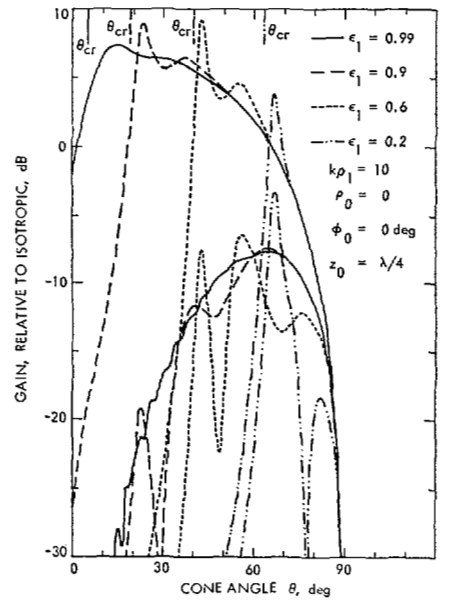

(a)

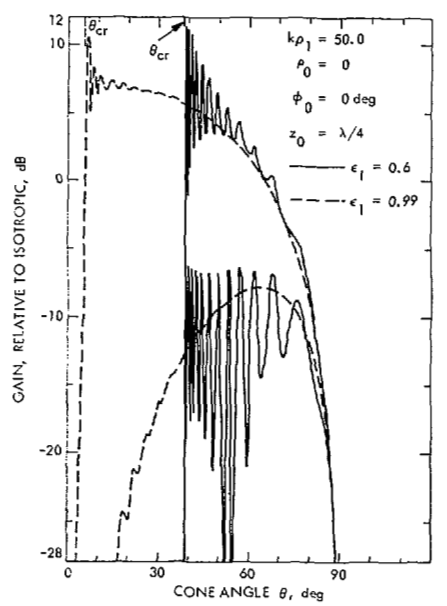

(b)

Fig. 3. Patterns in presence of plasma column for on-axis antenna.

tend towards corresponding ϵ_1 on-axis patterns for smaller $k\rho_1$. Patterns for $k\rho_1 = 50$ were not obtained since the calculation of each point would require as many as 200 terms in the series, and computation to include all peaks would be tedious. Moreover, the expected effect would be similar to that seen in the case of $k\rho_1 = 10$. It should be noted that for large $k\rho_1$ more convergent representations can be derived by applying a Watson transformation to the slowly convergent harmonic series (25) and (26), and evaluating the resultant integrals to obtain the geometrical optical approximation of the fields [6], [9].

The results shown in Figs. 3 and 4 cover the situation when the plasma is transparent ($\epsilon_1 > 0$). When the plasma is opaque ($\epsilon_1 < 0$), the fields are rapidly attenuated and radiation due to space waves is negligible. This represents

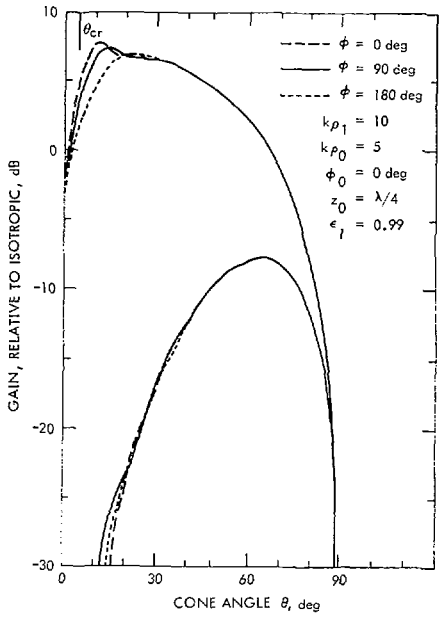

(a)

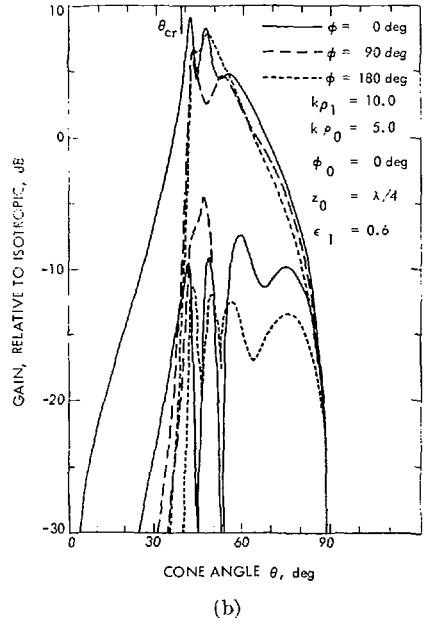

(b)

Fig. 4. Patterns in presence of plasma column for off-axis antenna.

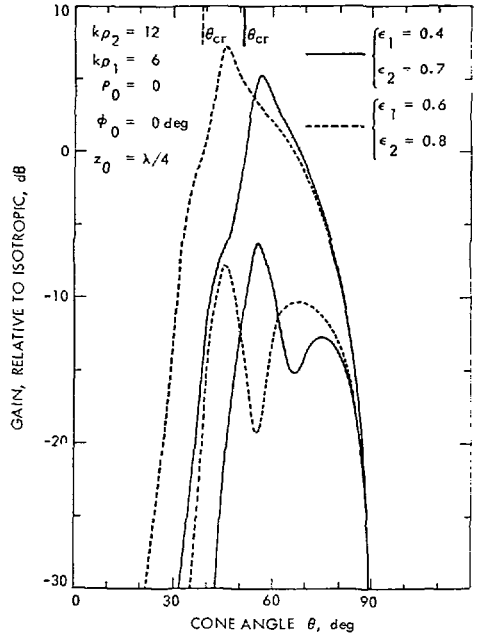

Fig. 5. Patterns in presence of plasma shell with far-wake approximation.

the situation when radio blackout occurs. When the plasma is opaque, surface waves may be supported by the plasma column. The dispersion relations for these surface waves have been studied elsewhere [10]. A single mode exists for each value of n and the maximum frequency limit is $\omega = \omega_p/\sqrt{2}$, where ω_p is the electron plasma frequency. Determination of the power carried by the surface wave is straightforward [11], but will not be carried out in this paper. Physical arguments indicate that the contribution in the far field from the surface wave is very small and can be neglected. The power carried by a surface wave is radiated only at discontinuities in the plasma column. Since few discontinuities exist in the ionized wake, the surface wave will propagate along the wake and slowly decay because of losses and very little radiation will take place. Another point to be considered for surface waves is the efficiency with which they are generated. The surface wave field decays away from the free-space interface both in the free-space and plasma regions. The result of this is that the surface wave will be excited with maximum efficiency when the antenna is located close to the free-space interface. For cases of large $k\rho_1$, the efficiency of surface wave excitation is therefore often quite low [11].

B. Shell Configuration

In the near wake of a blunt-body capsule, the electron density is maximum at the edge of the wake because of the normal bow shock. We will therefore examine the shell configuration for which ϵ_1 is greater than ϵ_2 and call this the near-wake case. At larger distances behind the capsule, the electron density will be maximum on the z axis and will monotonically decrease for increasing radial distance. In this case ϵ_1 is less than ϵ_2 and we will call this the far-wake case.

1) *Far-Wake Case*: Radiation patterns for two cases are shown in Fig. 5. When these patterns are compared with those obtained for the column configuration (Fig. 3), it is seen that the addition of the plasma shell smoothens the column patterns. The respective critical cone angles θ_{cr} calculated from Snell's law and applied to the medium of higher electron density region 1 are also shown in Fig. 5. The patterns are seen to begin their descent in the proximity of these critical angles.

2) *Near-Wake Case*: The patterns shown in Fig. 6 are typical of those obtained for the near-wake configuration. The critical cone angle calculated from application of Snell's law to the medium of higher electron-density region 2 is also shown. As in the far-wake region, the patterns decrease rapidly with decreasing cone angle for

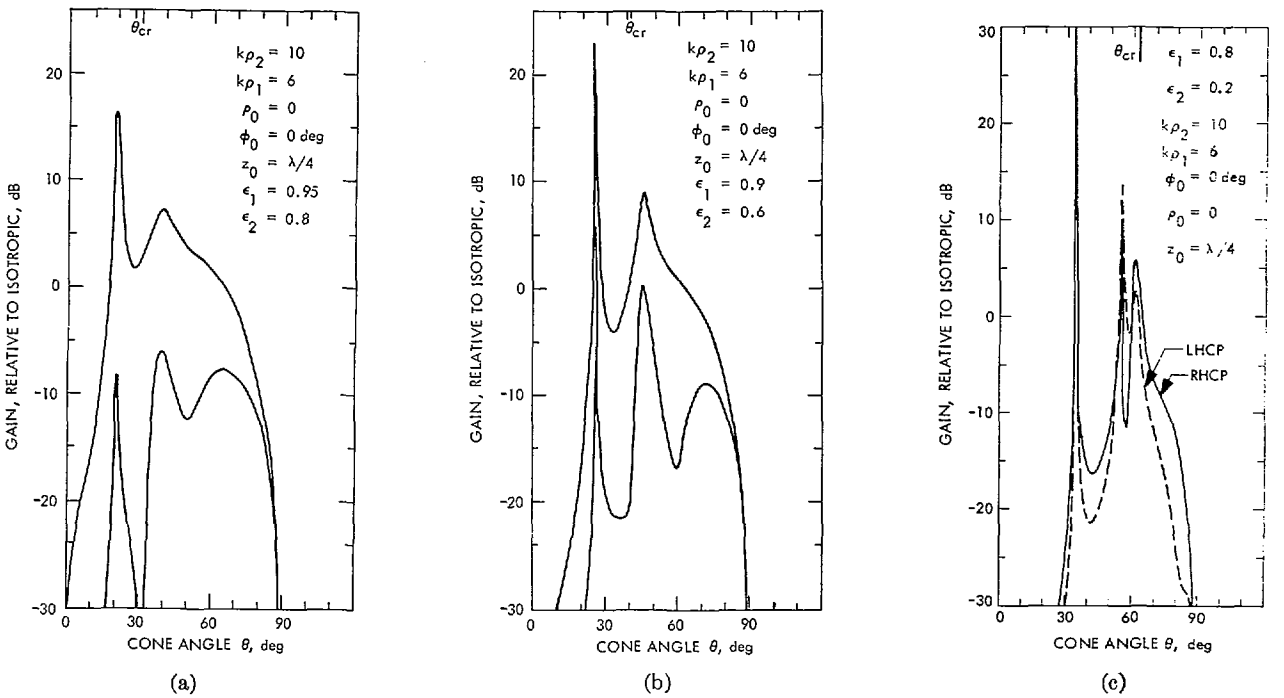

Fig. 6. Patterns in presence of plasma shell with near-wake approximation.

cone angles less than θ_{cr}. In addition, there are sharp peaks present. These peaks are due to leakage of trapped energy and have been observed in other studies [12]–[14]. The physical picture can be described as follows. If radius ρ_2 is extended to infinity, a surface wave is excited along ρ_1. When ρ_2 is finite, this surface wave continues to propagate along ρ_1 with part of its energy leaking away at ρ_2. Since the surface decays exponentially in the radial direction before it appears at ρ_2, its amplitude at ρ_2 is small and the leakage of energy is small too. Since the surface wave is a fast wave, the leaky-wave pole can be very close to the saddle point resulting in a sharp peak in the radiation patterns. If β is the propagation constant of the surface wave, the location of the leaky-wave peak is given approximately by $\sin^{-1}(\beta/k)$ [15].

In Fig. 6 it can be seen that as electron density increases the leaky-wave peak becomes sharper and shifts to larger cone angles. In Fig. 6(c) the electron density is sufficiently dense that a higher order leaky-wave mode is generated and this accounts for the additional peak at $\theta = 55.7$ degrees. Patterns other than those shown in Fig. 6 were obtained and a summary of the leaky-wave peaks is given in Table I. If $k\rho_1$ is constant and $k\rho_2$ allowed to increase, the radiated energy is reduced and the peak becomes sharper. When the location of a constant thickness plasma shell (region 2) is allowed to increase radially, the leaky-wave peak shifts to smaller cone angles and the peak becomes sharper.

The patterns of Figs. 5 and 6 are for the case when the antenna is located on axis. If the antenna is moved off axis, the general effects are similar to those observed in the column case (Fig. 4). However, in the near-wake configuration moving the antenna off axis would generate higher order surface wave modes. Consequently, additional peaks for cone angles less than θ_{cr} will appear in the patterns. Since the power carried by these higher order modes is relatively small, the magnitude of the corresponding leaky-wave peaks will be small too [see Fig. 6(c)]. When $k\rho_1$ and $k\rho_2$ are increased, more peaks will develop in the patterns for cone angles greater than θ_{cr} as in the column case and the drop in the proximity of θ_{cr} will become sharper. Additional leaky-wave peaks may occur for cone angles less than θ_{cr} in the near-wake configuration since higher order surface wave modes may be excited.

For similar physical reasons given for the column configuration, radiation in the far field is negligible when the plasma becomes opaque.

In this paper the wake has been approximated by a cylindrically stratified plasma consisting of N plasma regions. In an actual wake the variation of electron density is a continuous one. From the results of Figs. 3–6 it is seen that as plasma layers are added, the patterns remain similar but become smoother. The patterns still possess an on-axis null whose extent is proportional to the peak electron density in the wake. These results have been confirmed in a current separate study utilizing geometrical optics where the electron density is a slowly varying and continuous function of radius only.

For increasing axial distance behind the capsule there are 1) a decay in electron density, 2) a transition from near to far-wake regions, and 3) an expansion of wake radius. According to typical electron density profiles given in [4] these changes are rather slow and are therefore not expected to significantly alter the results of Figs. 3–6. Another point worth mentioning is that other than the leaky-wave peaks that appear in the null region the pat-

TABLE I
SUMMARY OF LEAKY-WAVE PEAKS

$k\rho_1$	$k\rho_2$	Location of Peak Cone Angle (degrees)	Gain of Peak (dB)
4	6	31.72	12.52
4	8	31.63	18.67
4	10	31.58	24.79
4	12	31.58	30.84
4	6	31.72	12.52
6	8	26.4	15.2
8	10	23.7	16.9
10	12	22.2	17.98

terns for the near-wake configuration are comparable to those of the far-wake configuration for identical peak electron densities [compare for instance Figs. 5 and 6(b)].

Although the rear of the capsule is finite, it has been represented in this paper by an infinite ground plane. Such an assumption is satisfactory for the following reasons. First of all, although the rear of the capsule is finite, it is large compared to wavelength. Secondly, it has been seen in this study that the patterns are affected the most in the broadside direction where refraction effects are most pronounced and the least in the endfire direction. Also, there is little radiation in the endfire direction to begin with. Therefore, the diffraction effects of the finite capsule can be neglected.

V. CONCLUSION

The effects of the ionized wake on a turnstile antenna operating at 400 and 2295 MHz prior to and after blackout have been studied. It is seen that for both near- and far-wake electron-density profiles the radiation patterns develop a conical null region. The extent of the null region is proportional to the peak electron density in the wake and can be predicted from Snell's refraction law. For the near-wake configuration, sharp peaks appear within the null region of the patterns. These peaks are attributed to leaky-wave radiation. Under blackout conditions surface waves may be generated along the wake. Physical reasons have been given to show that the contribution of surface waves to radiation is negligible. The effect of the conical null region in the patterns is to prolong blackout time for communication cone angles that lie within the null region. There are no serious depolarization effects in the non-null region and satisfactory communications can be carried out.

REFERENCES

[1] D. F. Spencer, "An evaluation of the communication blackout problem for a blunt Mars-entry capsule and a potential method for the elimination of blackout," Jet Propulsion Lab., California Institute of Technology, Pasadena, Tech. Rept. 32-594, April 1964.
[2] A. J. Kelly, "An experimental feasibility study of injectant materials to alleviate Mars-entry communications blackout," Jet Propulsion Lab., California Institute of Technology, Pasadena, Tech. Rept. 32-835, November 1965.
[3] A. J. Kliore, D. L. Cain, G. S. Levy, V. R. Eshleman, G. Fjeldbo, and F. D. Drake, "Occultation experiment: results of the first direct measurements of Mars' atmosphere and ionosphere," *Science*, vol. 149, pp. 1243–1248, 1965.
[4] R. A. Hayami, and R. I. Primich, "Wake electron density measurements behind hypersonic spheres and cones," General Motors Defense Res. Labs., Greenbelt, Md., Rept. TR67-01B, March 1967.
[5] J. R. Wait, *Electromagnetics and Plasmas*. New York: Holt, Rinehart and Winston, 1968.
[6] J. R. Wait, *Electromagnetic Radiation from Cylindrical Structures*. New York: Pergamon, 1959.
[7] R. E. Collin, *Field Theory of Guilded Waves*. New York: McGraw-Hill, 1960.
[8] G. L. Yip and S. R. Seshadri, "Radiation from an electric dipole in an axially magnetized plasma column–dipolar modes," *Can. J. Phys.*, vol. 45, pp. 3627–3648, November 1967.
[9] H. Bremmer, *Terrestrial Radio Waves*. Amsterdam: Elsevier, 1949.
[10] V. L. Granastein, S. P. Schlesinger, and A. Vigants, "The open plasmaguide in extremes of magnetic field," *IEEE Trans. Antennas and Propagation*, vol. AP-11, pp. 489–496, July 1963.
[11] S. R. Seshadri, "Radiation from an electric dipole in a plasma column," *Proc. IEE*, vol. 112, pp. 249–253, February 1965.
[12] A. Ishimaru, "The effect of unidirectional surface wave along a perfectly conducting plane on the radiation from a plasma sheath," in *Electromagnetic Aspects of Hypersonic Flight*, W. Rotman, H. K. Moore, and R. Papa, Eds. Washington, D.C.: Spartan, 1964, pp. 147–168.
[13] J. H. Harris, A. T. Villeneuve, and L. A. Broca, "Radiation patterns from plasma enclosed cylindrical hypersonic vehicles," *Radio Sci.*, vol. 69D, pp. 1335–1343, October 1965.
[14] J. H. Harris, "Leaky-wave beams of multiply layered plasma media," *Radio Sci.*, vol. 3, pp. 181–189, February 1968.
[15] H. O. Goldstone and A. A. Oliner, "Leaky-wave antennas, I: rectangular waveguides," *IRE Trans. Antennas and Propagation*, vol. AP-7, pp. 307–319, October 1959.